FERMILAB-PUB-16-285-A

DRAFT VERSION MAY 12, 2016
Preprint typeset using LaTeX style emulateapj v. 5/2/11

arXiv:1605.03183v1 [astro-ph.CO] 10 May 2016

# COSMIC REIONIZATION ON COMPUTERS. PROPERTIES OF THE POST-REIONIZATION IGM

NICKOLAY Y. GNEDIN[1,2,3], GEORGE D. BECKER[4], XIAOHUI FAN[5]

*Draft version May 12, 2016*

## ABSTRACT

We present a comparison between several observational tests of the post-reionization IGM and the numerical simulations of reionization completed under the Cosmic Reionization On Computers (CROC) project. We show that CROC simulations reproduce "out-of-the-box" the observed distributions of Gunn-Peterson optical depths, underscoring the importance of self-consistent modeling of radiative transfer. We also show that CROC simulations match well the observed distributions of dark gaps from SDSS quasars. Finally, we introduce a novel statistical probe of the small-scale structure in the IGM: heights and widths of transmission peaks. Simulations match the peak height distributions reasonably, but do not reproduce the observed abundance of wide peaks.

*Subject headings:* cosmology: theory – cosmology: large-scale structure of universe – methods: numerical – intergalactic medium

## 1. INTRODUCTION

The Lyman-$\alpha$ forest, the collective intervening absorption systems from the spectra of distant quasars, has always been seen as an excellent probe of the intergalactic medium (IGM). Ever since its discovery, it has been instrumental in exploring the history of the IGM; the presence of spectral regions with low absorption has provided the first evidence for the existence of hydrogen reionization era (Gunn & Peterson 1965). After that discovery, constraining the epoch of reionization became an important topic in cosmological research (Becker et al. 2015a).

A critical impact on the study of cosmic reionization with the Lyman-$\alpha$ forest has been made by the Sloan Dark Sky Survey (SDSS). A rapid rise in the flux decrement at $z \geq 5.7$ in the spectra of quasars discovered by SDSS (Becker et al. 2001; Fan et al. 2006) has been the first and remains the strongest evidence that the epoch of reionization lies not far beyond that redshift mark. Also, the distinct features of the $z \sim 6$ redshift QSO spectra - long, dark absorption gaps separated by isolated transmission peaks - implies that reionization has largely ended at that point. More recent surveys of high-redshift QSOs (Gallerani et al. 2008; Mortlock et al. 2011; Bolton et al. 2011; Bañados & Ferreira 2014; McGreer et al. 2015; Becker et al. 2015b), gammy ray bursts (Chornock et al. 2013), and high redshift galaxies (Stark et al. 2010; Pentericci et al. 2011; Treu et al. 2013; Schenker et al. 2014; Tilvi et al. 2014) strengthen this conclusion. Never-the-less, statistical properties of the Lyman-$\alpha$ forest in the very aftermath of cosmic reionization remain poorly explored. One of the reasons is that $z > 5$ Lyman-$\alpha$ forest spectra look like spectra of no other astrophysical object; beginning students often take these absorption spectra for emission ones, confused by the narrow transmission regions between heavily blended absorption. As the result, many classical methods of spectral analysis (fitting absorption features, flux power spectrum, etc) become unusable or uninformative. New statistical probes of this unique cosmic phenomenon have to be developed, but some guidance on where to start is needed.

That is where cosmological simulations can come to the aid, complementing in many respects the direct observations of the high redshift IGM. Many of modern simulations give reasonable predictions for the overall statistical properties of the IGM (c.f. the column density or line width distributions, flux power spectrum, etc) at lower redshifts. Of course, not any simulation is a suitable tool for interpreting the observational data - only those that reproduce the actual measurements well enough can be expected to provide an approximately correct physical model of reality.

In this paper we make a first small step in this direction, compare the statistical properties of the observed Ly-$\alpha$ forest with several sets of numerical simulations of reionization produced by the Cosmic Reionization On Computers (CROC) project (Gnedin 2014; Gnedin & Kaurov 2014). Our goal is two-fold: first, to check how well the simulations match the general properties of the observed universe, as a validation of the simulation approach; second, to identify discrepancies and limitations of the simulations, from which one can, potentially, learn important insights into the underlying physics of reionization.

This work should not be considered as a complete project or a self-contained effort. Provided the validation of the simulations against the observational constraints is acceptable, we will use simulations in the future as testing grounds for developing new statistical techniques and for exploring connections between observables and the properties of the underlying gas distribution.

## 2. SIMULATIONS AND OBSERVATIONAL SAMPLES

In this work we use simulations from the Cosmic Reionization On Computers (CROC) project (Gnedin 2014; Gnedin & Kaurov 2014). CROC simulations are designed to provide a physically reasonable and internally self-consistent model of reionization. They include a wide range of physical effects deemed necessary for modeling reionization correctly in cosmological hydrodynamic simulations, including star formation and stellar feedback, fully coupled 3D radia-

[1] Particle Astrophysics Center, Fermi National Accelerator Laboratory, Batavia, IL 60510, USA; gnedin@fnal.gov
[2] Kavli Institute for Cosmological Physics, The University of Chicago, Chicago, IL 60637 USA
[3] Department of Astronomy & Astrophysics, The University of Chicago, Chicago, IL 60637 USA
[4] Space Telescope Science Institute, 3700 San Martin Dr, Baltimore, MD 21218, USA
[5] Steward Observatory, University of Arizona, Tucson, AZ 85721

Operated by Fermi Research Alliance, LLC under Contract No. DE-AC02-07CH11359 with the United States Department of Energy.

tive transfer, non-equilibrium ionization of hydrogen and helium, radiation-field-dependent cooling and heating functions for the metal enriched cosmic gas, etc.

For this paper we use three independent realizations in $40h^{-1}$ Mpc boxes (runs B40.sf1.uv2.bw10.A-C from Gnedin (2014)). Simulations account for the DC mode (Gnedin et al. 2011) and, hence, properly model fluctuations up to the box size. These simulations achieve spatial resolution of up to 125 pc at $z = 6$ in physical units. The initial conditions are set on the uniform grid of $1024^3$, resulting in the Nyquist wavenumber of $k_{\rm Ny} = 80h\,{\rm Mpc}^{-1}$ (corresponding to about $0.55\,({\rm km/s})^{-1}$ in velocity units at $z = 6$), fully sufficient for modeling the Lyman-$\alpha$ forest even at lower redshifts.

For estimating numerical convergence, we also use a set of six realizations of a twice smaller, $20h^{-1}$ Mpc box (runs B20.sf1.uv2.bw10.A-F from Gnedin (2014)). Our science results, however, are all based on the $40h^{-1}$ Mpc runs.

For comparison with observations, we use two sets of data: flux probability distributions averaged over sightline segments ("skewers") of comoving $50h^{-1}$ Mpc from Becker et al. (2015b) and the spectroscopic sample of SDSS quasars at $5.7 < z < 6.4$ from Fan et al. (2006) and Becker et al. (2015b). The sample from Fan et al. (2006) includes 19 luminous quasars with high S/N, moderate resolution spectroscopy. Twelve in the sample were observed using the Echellette Imaging Spectrograph (ESI) on Keck-II telescope. The ESI data have a spectral resolution between 2000 and 6000 (depending on the slit used during the observations). The rest of the spectra were observed on the MMT, HET and Kitt Peak 4-meter Telescopes, with spectral resolution of $R \sim 1000$. Details of this dataset can be found in Fan et al. (2006).

To complement the data from Fan et al. (2006), we also use 7 quasar spectra from Becker et al. (2015b) that were also obtained with ESI on Keck or X-Shooter on VLT with similar spectral resolution to the SDSS data.

Flux probabilty distributions have been measured by Becker et al. (2015b) from a sample of quasar absorption spectra that includes 19 $z > 5.7$ quasars from Fan et al. (2006) as well as 7 additional objects at $z > 5.8$ from the Pan-STARRS1 survey (Bañados et al. 2014).

## 3. RESULTS

### 3.1. *Distribution of Optical Depth*

The simplest statistical description of any data is a one-point statistics, or the Probability Distribution Function (PDF). Since the transmitted flux along the quasar sightline is a stochastic field, the flux PDF depends on the smoothing scale for the spectrum. Thermal broadening provides the minimum possible smoothing scale for the transmitted flux, and it would be the ideal smoothing scale to use. Unfortunately, few observational data exist at such high spectral resolution.

Recently, Becker et al. (2015b) published the flux PDF averaged over sightline segments ("skewers") of comoving $50h^{-1}$ Mpc in length in several redshift bins all the way to $z \approx 6$. While it is a less detailed probe of the post-reionization IGM than a PDF of a fully resolved spectrum, the distance of comoving $50h^{-1}$ Mpc is still less than the mean free path for an ionizing photon at $z < 6$ (Songaila & Cowie 2010), and, hence, is a sensitive probe of the fluctuations in the ionization state of the IGM, as has been demonstrated in Becker et al. (2015b).

Figure 1 shows the comparison of CROC simulations

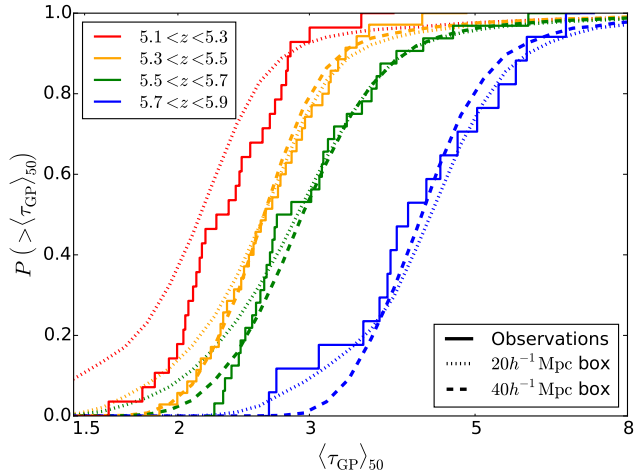


FIG. 1.— Probability Distribution Functions for the effective IGM opacity in $50h^{-1}$ Mpc skewers from our simulations (dotted and dashed lines) and observations of Becker et al. (2015b, solid lines).

to the Becker et al. (2015b) measurement in four redshift bins. While the size of our largest simulation boxes is only $40h^{-1}$ Mpc, a random line of sight crossing a periodic box remains a fair sample of the underlying matter distribution and free of artifacts due to boundary conditions up to 5 box lengths (Dall'Aglio & Gnedin 2010), so even our $20h^{-1}$ Mpc boxes are suitable for comparing with Becker et al. (2015b) measurements, although significantly smaller box sizes would not be adequate. We show both $20h^{-1}$ Mpc and $40h^{-1}$ Mpc simulation sets in Figure 1 to demonstrate a high degree of convergence of the numerical results. The agreement with the observational data remains excellent all the way to $z = 5.3$, but deteriorates somewhat at lower redshifts. This is not surprising - as Gnedin (2014) demonstrated, CROC simulations match the observed galaxy UV luminosity functions well for all redshifts $z \geq 6$, but overpredict the faint end slope at $z = 5$. Hence, at $z \sim 5$ there are more ionizing photons in the simulation than in reality, and the IGM in the simulations becomes over-ionized.

The agreement between our simulations and the data is genuine, the Becker et al. (2015b) data were not available when the simulations we completed. However, some degree of tuning in the simulations is, indeed, present.

As has been shown in Gnedin (2014), the emission of ionizing radiation by model galaxies is controlled by a single parameter $\epsilon_{\rm UV}$, the "escape fraction of ionizing radiation up to the simulation resolution". The parameter $\epsilon_{\rm UV}$ encapsulates our ignorance about several important properties of real galaxies in the reionization era, such as the stellar IMF, the duration of the embedded stage of star formation, etc. Note, however, that since CROC simulations are reaching spatial resolution of the order of 100 pc, they are able to model the actual escape of ionizing radiation from the resolution scale to larger scales. The absorption of ionizing radiation from the stellar surface to the resolution limit (for example, absorptions inside a parent molecular cloud) is not resolved, and, hence, is also encapsulated into the $\epsilon_{\rm UV}$ parameter. This parameter cannot be deduced from the first principles yet, and has to be fixed by comparing with observational data.

In the simulations we use in this paper, the $\epsilon_{\rm UV}$ parameter has been fixed by comparing simulations to the mean Gunn-Peterson optical depth from SDSS quasars (Fan et al. 2006).

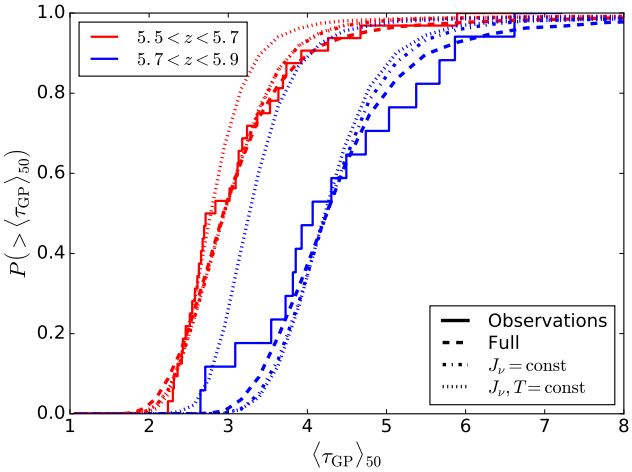


FIG. 2.— Effect of physical assumptions on the PDF for the effective IGM opacity (we only show the last two redshift bins where the effect is the largest for the sake of clarity). Solid and dashed lines are the same as in Fig. 1 (data and the fully self-consistent simulations). Dot-dashed lines show a distribution computed from the simulation snapshots under the assumption of ionization equilibrium and uniform ionizing background, while dotted lines also add an assumption of isothermal IGM with $T = 20{,}000$ K. In the latter two cases the value of the uniform ionizing background is adjusted to match the value of $\langle \tau_{50} \rangle$ at which PDF=0.5; the second set of dotted lines have the values of the uniform ionizing background adjust to match the lowest two panels of Fig. 11 from Becker et al. (2015b). Modified, non-self-consistent models provide significantly worse fits to the data.

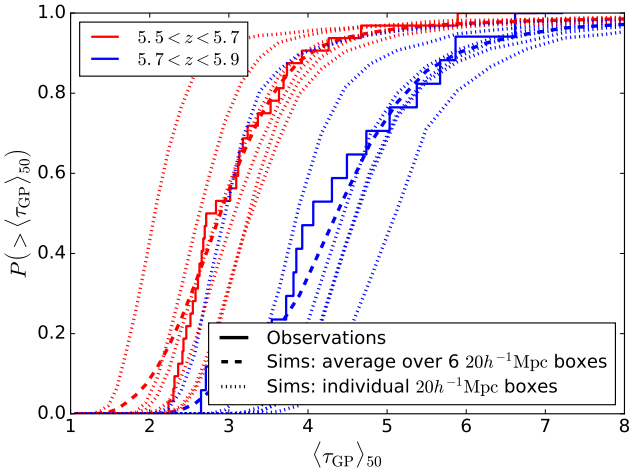


FIG. 3.— Effect of cosmic variance in small simulation volumes on the PDF for the effective IGM opacity. Each of the pairs of dotted lines (two lines for two redshift bins) are from one of 6 independent realizations of our $20h^{-1}$ Mpc box (see §2), while the dotted lines show the global averages over these 6 realizations. The main reason in the wide spread of the observed opacities is in cosmic variance on scales above $20h^{-1}$ Mpc.

That choice turned out to provide the excellent fit to Becker et al. (2015b) data as well. We also note that the agreement with data is obtained without any need for rare sources or large temperature variations, as has been suggested recently in some studies (D'Aloisio et al. 2015; Chardin et al. 2015), and in simulations volumes of modest sizes, contrary to conclusions of Davies & Furlanetto (2015). Hence, our success in matching the observations emphasizes the importance of modeling reionization self-consistently, in a fully coupled manner (i.e. with radiative transfer followed simultaneously, and at the same spatial resolution, as gas dynamics and star formation).

In order to illustrate the importance of modeling radiative transfer self-consistently further, we show in Figure 2 PDF for modified synthetic spectra, in which, first, the ionizing background is assumed to be uniform and, second, the IGM is taken to be isothermal. We find the temperature effect to be small, but the non-uniformity of the ionizing background to be significant. We also note that the difference between the data and the model with uniform ionizing background and IGM temperature (the so-called "density-variation-only" model) appears to be less in Fig. 2 than in Fig. 11 of Becker et al. (2015b) when we normalize the value for the uniform ionizing background so that the model and the data have he same values of $\langle \tau_{50} \rangle$ at which PDF=0.5. To show that we do fully reproduce results of Becker et al. (2015b), the second (leftmost) set of dotted lines in Fig. 2 show different normalization for the uniform ionizing background that match exactly the two lowest panels of Fig. 11 from Becker et al. (2015b).

Finally, in Figure 3 we illustrate the effect of cosmic variance on large scales on the width of the observed distribution. In each of our smallest, $20h^{-1}$ Mpc boxes, the PDF for the effective opacity is significantly narrower than in the observations, and is similar in shape to that found in (Chardin et al. 2015) (see their Fig. 14). However, the average over all 6 realizations is much wider and is reasonably consistent with the data. Hence, we can conclude that the primary reason for the wide distribution of the effective IGM opacity in the observations is due to cosmic variance on scales above $20h^{-1}$ Mpc.

### 3.2. *Statistics of Dark Gaps*

Going beyond PDFs, two-point statistics (power spectrum, correlation function) often used in studies of the large scale structure and the Lyman-$\alpha$ forest at intermediate redshifts ($z \sim 2-4$). The transmitted flux in the spectra of high redshift quasars ($z \gtrsim 5$) is so far from a Gaussian random field, however, that these statistics include only a small amount of information about the distribution of neutral gas in the universe. Hence, traditionally other, more sophisticated statistical probes have been used to explore the forest in the very aftermath of cosmic reionization.

One such probe is the distribution of dark gaps (continuous regions of low flux). It has been measured observationally in great detail (Fan et al. (2006)) and has also been used as an effective indicator for comparison of observations and simulations (Paschos & Norman 2005). It provides a natural description of statistical properties of high redshift Lyman-$\alpha$ spectra (which mostly contain single transmission spikes separated by dark gaps of various lengths) and shows well the drastic evolution in absorption between $z \approx 5.5$ and $z \approx 6$.

Following the definition of dark gaps from Songaila & Cowie (2002) and Fan et al. (2006), we analyze the distribution of dark gaps in our simulation sets and compare it to the sample of 12 Sloan Digital Sky Survey (SDSS) quasars from Fan et al. (2006). We select only quasars obtained with the Keck ESI instrument to have uniform spectral sampling and noise properties in the data sample.

In order to make the comparison between the observations and the simulations more realistic, we add noise to synthetic spectra sampled directly from the observational measurements. Specifically, at each simulation snapshot we measure the rms noise in all observed spectra that cover the snapshot redshift in the redshift interval $\Delta z = \pm 0.1$ around the snapshot epoch and add noise values from different observed sightlines in quadratures. We then add Gaussian noise with

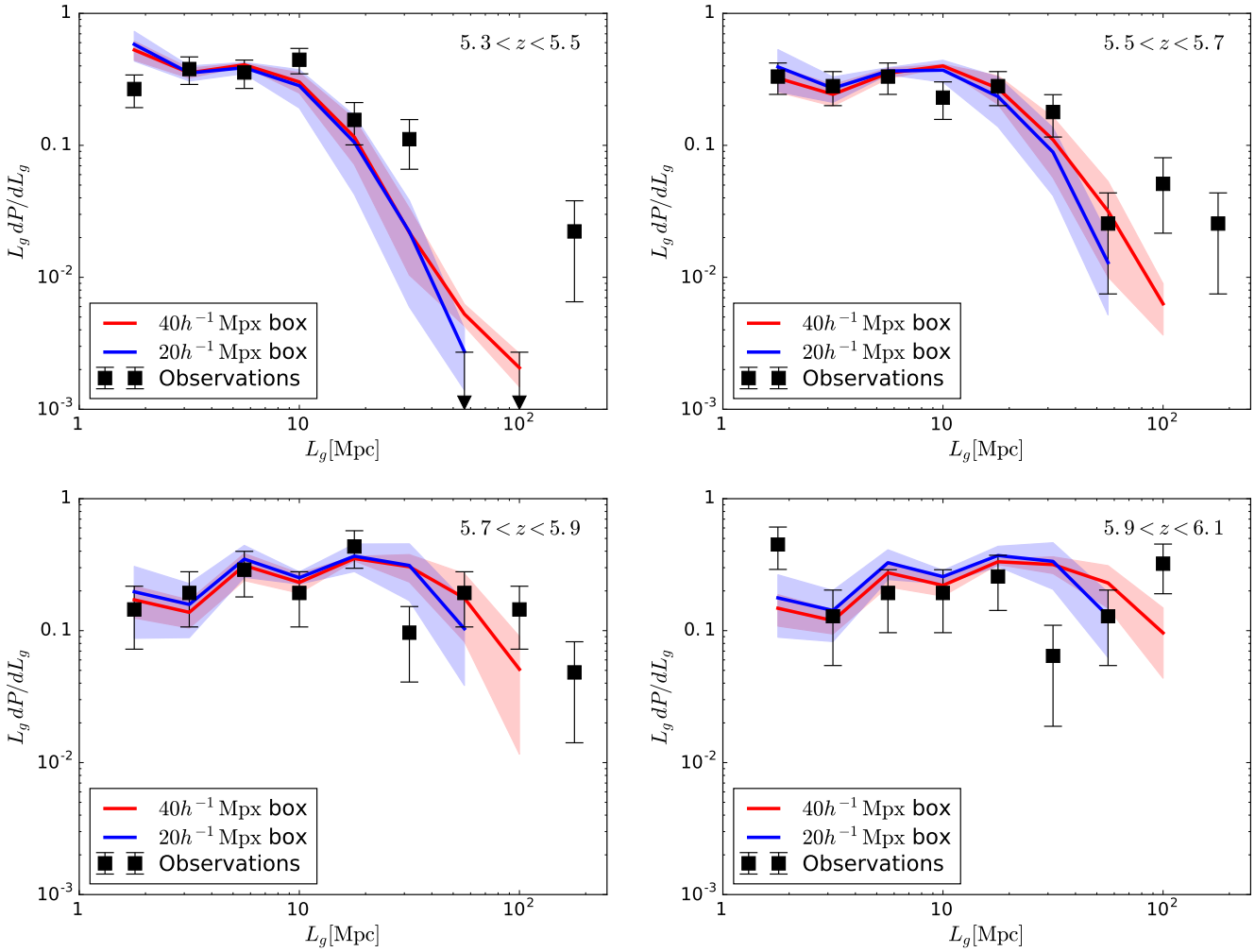


FIG. 4.— Distribution of dark gaps for two simulation sets with different box sizes and the observational data from SDSS. Shaded bands show the error of the mean for the simulated results.

the observed rms to all synthetic spectra.

Observed spectra come with slightly variable spectral resolution at different wavelength. To make spectral resolution between simulations and data exactly the same, we smooth both real and synthetic spectra with the same top-hat filter of uniform resolution $R \equiv \lambda/\Delta\lambda = 2000$, which is approximately the lowest common resolution of all observed spectra. The reason for using a top-hat filter rather than, say, a Gaussian one, is that the top-hat smoothing is independent of any prior smoothing (i.e. smoothing a $R = 3000$ spectrum with $R = 2000$ resolution results in the $R = 2000$ spectrum), while in Gaussian smoothing window widths add in quadratures, and hence any prior smoothing needs to be known precisely.

Spectral gap statistics uses a single parameter - the threshold value that specifies what "low flux" means. This value is commonly quantified by the effective optical depth $\tau_{\rm min}$ - a contiguous region in the spectrum with flux $F < \exp(-\tau_{\rm min})$ is considered to be a single dark gap. We use the value of $\tau_{\rm min} = 2.5$ as the fiducial value, to be consistent with Fan et al. (2006).

Figure 4 shows the comparison of dark gaps in four different redshift ranges between our simulations and the SDSS data (we do not show the $5.1 < z < 5.3$ redshift range that is not covered by the quasars in the observational sample). In order to make the comparison between a few long lines of sight from observations data and a large number of relatively short lines of sight from the simulations meaningful, we plot the differential probability $L_g d/dL_g P$ to find a dark gap of a given comoving length between $L_g$ and $L_g + dL_g$ along a given sightline. Operationally, for a given number of sightlines, we find the number $\Delta N(L_g, \Delta L_g)$ of gaps that fall in a bin of length $\Delta L_g$ around $L_g$, and define

$$\frac{dP}{dL_g} = \frac{\Delta N(L_g, \Delta L_g)}{N_{\rm tot}\Delta L_g},$$

where $N_{\rm tot}$ is the total number of all gaps (of any length), so that $dP/dL_g$ is normalized to unity,

$$\int \frac{dP}{dL_g}\, dL_g = 1.$$

With such definition, $dP/dL_g$ is independent of the bin size $\Delta L_{\rm gap}$) in the limit of many sightlines and small bins.

Lengths of dark gaps in the simulations are limited by the finite sizes of computational boxes, and that restricts the dynamic range of curves plotted in Figure 4, which is especially apparent for the smaller, $20h^{-1}$ Mpc boxes. Overall, the agreement between simulations and observations is good in all four redshift ranges, although it appears to get slightly worse in the lowest redshift bin. The apparent discrepancy can be caused

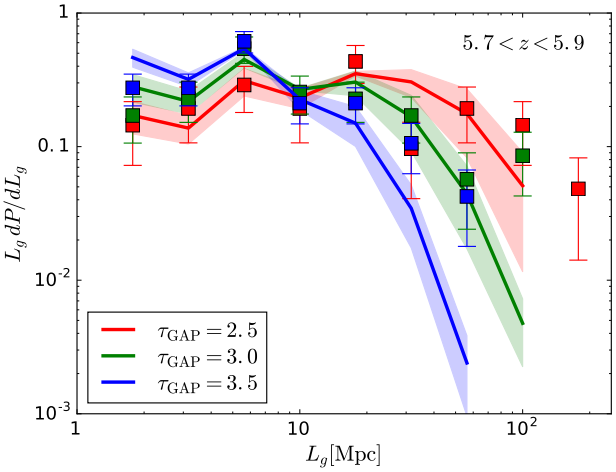


FIG. 5.— Distribution of dark gaps in the redshift interval $5.5 < z < 5.7$ for three different values of the threshold $\tau_{\rm min}$.

by small number statistics (the last bin in the top left panel includes just 1 gap), but also can be genuine, consistent with the limitation of CROC simulations discussed above.

We also explore the effect of varying the dark gap threshold $\tau_{\rm min}$ on the overall gap distribution in Figure 5. As could be expected, as the flux threshold $\exp(-\tau_{\rm min})$ is being lowered, longer gaps split into shorter ones, shrinking the tail of the distribution toward lower values. However, the overall shape of the distribution does not change that much.

### 3.3. *Statistics of Transmission Peaks*

While dark gap distribution is a powerful tool that has been successfully used to characterize the post-reionization IGM, it has its limitation. First, it provides little information on the density distribution in the IGM, as most densities except the lowest ones would produce dark gaps at $z \sim 6$. Second, transmission peaks that separate gaps are treated just as walls, with no significance given to the peak height (besides it is being above the threshold) or its width. Hence, the distribution of transmission peak heights and widths may serve as a complementary statistics.

In order to explore this new statistical test of the post-reionization IGM, we define as a "peak" a continuous segment of the spectrum, such that for all pixels in the segment the normalized flux is above $\alpha h_p$, where $h_p$ is the maximum normalized flux value inside the segment. The width of the segment $w_p$ is then identified with the "width of the peak". The value of $\alpha$ could be signal-to-noise dependent, but in this pilot study we choose a fixed threshold of $\alpha = 0.5$, so that the peak width is the familiar Full Width at Half Maximum (FWHM). That particular choice is entirely empirical, and we find that within the reasonable range (if $\alpha$ is not too small), the threshold value $\alpha$ affects the peak height and width statistics rather little (besides a trivial rescaling of widths). To avoid including noise, we only consider a peak to be real if it is wider than one resolution element and has a signal-to-noise ratio of at least 3.

In Figure 6 we present the peak height and width distributions as 2D histograms, both for the SDSS observational data and for our $40h^{-1}$ Mpc simulation set, in four redshift intervals. Since quasars affect their own environments within their "proximity zones", the ionization state of the gas near quasars is expected to be different from the general IGM. In order to check for that effect, we show in Fig. 6 peaks within and outside the quasar proximity zones with different symbols. Sizes of proximity zones for for the sample we study in this paper were measured by Carilli et al. (2010); we use their values for all quasars in the sample except for J1306+0356, where visual examination of the data indicates that the proximity zone extends to 10 Mpc, beyond the value of 6 Mpc quoted by Carilli et al. (2010). The proximity effect is glaring at $z \sim 6$, but is much less pronounced at $z \sim 5.5$.

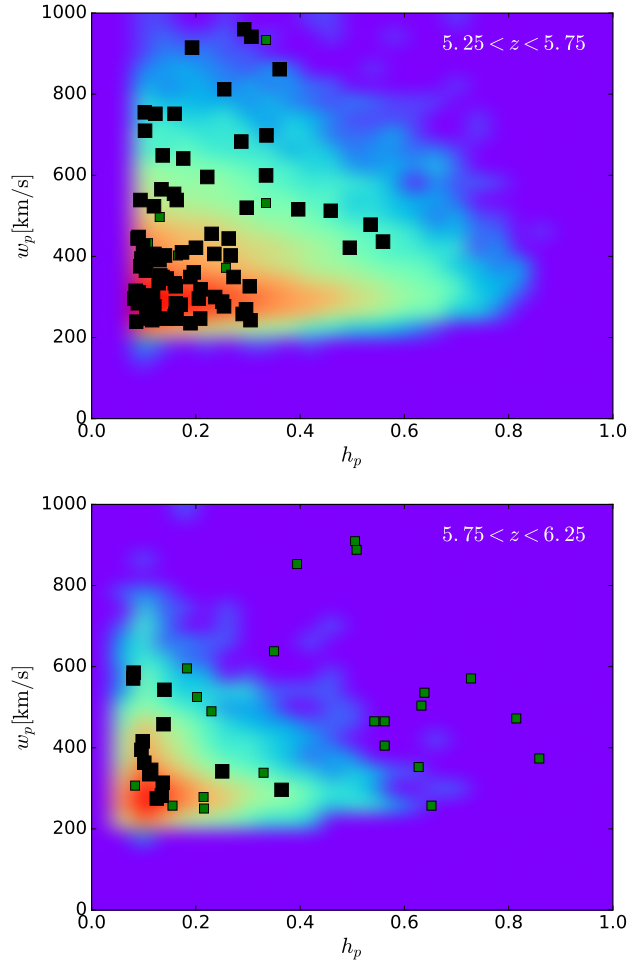


FIG. 6.— Two-dimensional distributions of transmission peaks and widths in the simulations (colored images) and the data (squares). Larger black squares show observed peaks outside the proximity zones of their quasars, while smaller green squares are for peaks inside the quasar proximity zones.

A more quantitative comparison of these distributions is offered in Figure 7, which shows one dimensional (i.e. projected along one of the two axes) probability distributions for peak heights and widths. While the peak heights are reproduced faithfully (within the observational uncertainties) by the simulations, there is a significant lack of wide peaks in the synthetic spectra. This discrepancy cannot be attributed to the limited volumes of CROC simulations - for both distributions the differences in the simulation volume are much smaller than the magnitude of the discrepancy. We also note that observed spectra have spectral resolution better than $R = 2000$, so transmission peaks with $w_p > 800$ km/s are well resolved; hence, the discrepancy we find cannot be attributed to instrumental effects and is genuine.

## 4. CONCLUSIONS

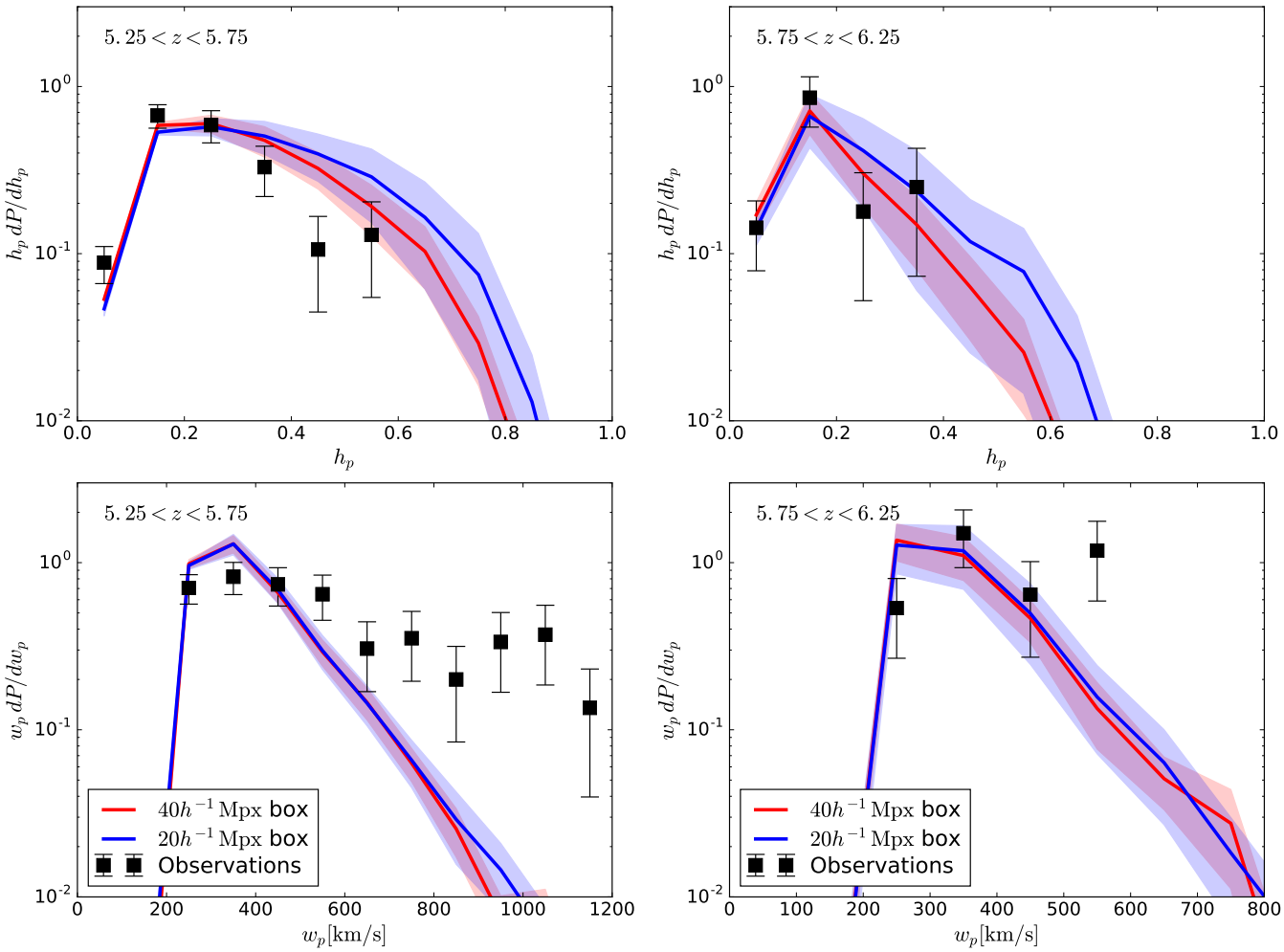


FIG. 7.— One-dimensional probability distributions for peak heights and widths in the two redshift bins in two simulation sets and in the data. Shaded bands show the error of the mean for the simulated results. The discrepancy at large $w_p$ is real and is not caused by the limited sizes of the simulation volumes.

Statistical properties of the Lyman-$\alpha$ forest in high redshift ($z \gtrsim 5$) quasar spectra is a barely touched, full of unexplored potential research subject. Spatial variations of the transmitted flux in the spectra contain rich information on the physics of the IGM and the cosmological density distribution, as well as on the large-scale clustering properties of reionizing sources. In this exploratory work we have made a modest attempt at accessing this information, and compared CROC simulations with some of the existing the observational data on high redshift quasars.

Besides applying the commonly used statistical tests: the PDF for the large-scale opacity (most sensitive to the large-scale distribution of ionizing sources) and the dark gap distribution (most sensitive to the large-scale matter clustering), we also introduce a new statistical probe of the small-scale structure in the IGM: heights and widths of transmission peaks. While CROC simulations match the large-scale statistical tests of the observational data reasonably well, and also provide a good match for the distribution of peak heights, there is a notable lack of wide peaks in the simulated spectra. The source of this discrepancy remains unclear at present. One possible reason is proximity zones around foreground quasars. While we exclude all transmission peaks within the proximity zones of targeted quasars, a sightline can also traverse a proximity zone around a foreground quasar, which would create a broad transmission spike. In CROC simulations quasars are included only as a global background, and, hence, individual proximity zones are not modeled. Another potential source of discrepancy is a limited simulated volume. While Fig. 7 shows little dependence on the simulation box size, with only two sampled box sizes the concordance may be accidental and simulations may, in fact, underpredict the abundance of large peaks. Exploring this discrepancy fully will require a substantial amount of effort for an uncertain benefit (surely, no one is going to claim that our simulations present the final truth, thus, discrepancies with the data are expected), and, therefore, we do not proceed with that effort at present.

An interesting avenue of further research is to use numerical simulations to understand better what physical properties of the IGM control the shapes of transmission peaks. For example, one may discover in the future that transmission peaks of particular heights and width are especially sensitive to some physical parameters, like gas density, ionization state, temperature, or the local ionization rate. Only in that case an effort for better modeling the peaks of those particular properties will be warranted.

Fermilab is operated by Fermi Research Alliance, LLC,

under Contract No. DE-AC02-07CH11359 with the United States Department of Energy. This work was also supported in part by the NSF grant AST-1211190. Simulations used in this work have been performed on the National Energy Research Supercomputing Center (NERSC) supercomputers "Hopper" and "Edison" and on the Argonne Leadership Computing Facility supercomputer "Mira". An award of computer time was provided by the Innovative and Novel Computational Impact on Theory and Experiment (INCITE) program. This research used resources of the Argonne Leadership Computing Facility, which is a DOE Office of Science User Facility supported under Contract DE-AC02-06CH11357. This work made extensive use of the NASA Astrophysics Data System and `arXiv.org` preprint server.

REFERENCES

Bañados, E., Venemans, B. P., Morganson, E., Decarli, R., Walter, F., Chambers, K. C., Rix, H.-W., Farina, E. P., Fan, X., Jiang, L., McGreer, I., De Rosa, G., Simcoe, R., Weiß, A., Price, P. A., Morgan, J. S., Burgett, W. S., Greiner, J., Kaiser, N., Kudritzki, R.-P., Magnier, E. A., Metcalfe, N., Stubbs, C. W., Sweeney, W., Tonry, J. L., Wainscoat, R. J., & Waters, C. 2014, AJ, 148, 14

Bañados, M. & Ferreira, P. G. 2014, Physical Review Letters, 113, 119901

Becker, G. D., Bolton, J. S., & Lidz, A. 2015a, ArXiv e-prints

Becker, G. D., Bolton, J. S., Madau, P., Pettini, M., Ryan-Weber, E. V., & Venemans, B. P. 2015b, MNRAS, 447, 3402

Becker, R. H., Fan, X., White, R. L., Strauss, M. A., Narayanan, V. K., Lupton, R. H., Gunn, J. E., Annis, J., Bahcall, N. A., Brinkmann, J., Connolly, A. J., Csabai, I., Czarapata, P. C., Doi, M., Heckman, T. M., Hennessy, G. S., Ivezić, Ž., Knapp, G. R., Lamb, D. Q., McKay, T. A., Munn, J. A., Nash, T., Nichol, R., Pier, J. R., Richards, G. T., Schneider, D. P., Stoughton, C., Szalay, A. S., Thakar, A. R., & York, D. G. 2001, AJ, 122, 2850

Bolton, J. S., Becker, G. D., Raskutti, S., Wyithe, J. S. B., Haehnelt, M. G., & Sargent, W. L. W. 2011, ArXiv e-prints

Carilli, C. L., Wang, R., Fan, X., Walter, F., Kurk, J., Riechers, D., Wagg, J., Hennawi, J., Jiang, L., Menten, K. M., Bertoldi, F., Strauss, M. A., & Cox, P. 2010, ApJ, 714, 834

Chardin, J., Haehnelt, M. G., Aubert, D., & Puchwein, E. 2015, ArXiv e-prints

Chornock, R., Berger, E., Fox, D. B., Lunnan, R., Drout, M. R., Fong, W.-f., Laskar, T., & Roth, K. C. 2013, ApJ, 774, 26

Dall'Aglio, A. & Gnedin, N. Y. 2010, ApJ, 722, 699

D'Aloisio, A., McQuinn, M. J., & Trac, H. 2015, ArXiv e-prints

Davies, F. B. & Furlanetto, S. R. 2015, ArXiv e-prints

Fan, X., Strauss, M. A., Becker, R. H., White, R. L., Gunn, J. E., Knapp, G. R., Richards, G. T., Schneider, D. P., Brinkmann, J., & Fukugita, M. 2006, AJ, 132, 117

Gallerani, S., Ferrara, A., Fan, X., & Choudhury, T. R. 2008, MNRAS, 386, 359

Gnedin, N. Y. 2014, ApJ, 793, 29

Gnedin, N. Y. & Kaurov, A. A. 2014, ApJ, 793, 30

Gnedin, N. Y., Kravtsov, A. V., & Rudd, D. H. 2011, ApJS, 194, 46

Gunn, J. E. & Peterson, B. A. 1965, ApJ, 142, 1633

McGreer, I. D., Mesinger, A., & D'Odorico, V. 2015, MNRAS, 447, 499

Mortlock, D., Warren, S., Patel, M., Venemans, B., McMahon, R., Hewett, P., Simpson, C., Theuns, T., Rottgering, H., Kuiper, R., Bolton, J., & Harhnelt, M. 2011, in Galaxy Formation, 88

Paschos, P. & Norman, M. L. 2005, ApJ, 631, 59

Pentericci, L., Fontana, A., Vanzella, E., Castellano, M., Grazian, A., Dijkstra, M., Boutsia, K., Cristiani, S., Dickinson, M., Giallongo, E., Giavalisco, M., Maiolino, R., Moorwood, A., Paris, D., & Santini, P. 2011, ApJ, 743, 132

Schenker, M. A., Ellis, R. S., Konidaris, N. P., & Stark, D. P. 2014, ApJ, 795, 20

Songaila, A. & Cowie, L. L. 2002, AJ, 123, 2183

—. 2010, ApJ, 721, 1448

Stark, D. P., Ellis, R. S., Chiu, K., Ouchi, M., & Bunker, A. 2010, MNRAS, 408, 1628

Tilvi, V., Papovich, C., Finkelstein, S. L., Long, J., Song, M., Dickinson, M., Ferguson, H. C., Koekemoer, A. M., Giavalisco, M., & Mobasher, B. 2014, ApJ, 794, 5

Treu, T., Schmidt, K. B., Trenti, M., Bradley, L. D., & Stiavelli, M. 2013, ApJ, 775, L29